JOURNAL OF AIRCRAFT
Vol. 41, No. 2, March–April 2004

Vibration Prediction for Rotor System with Faults Using Coupled Rotor-Fuselage Model

Mao Yang* and Inderjit Chopra†
University of Maryland, College Park, Maryland 20742
and
David J. Haas‡
Naval Surface Warfare Center, West Bethesda, Maryland 20817

A coupled rotor-fuselage vibration analysis is formulated to analyze the effect of rotor system faults on fuselage vibrations and rotor-blade displacements in both hover and forward-flight conditions. Two groups of rotor-system faults, adjustable and nonadjustable component faults, are modeled. Results are presented for an SH-60 helicopter and are compared with available flight-test data. A detailed aeroelastic analysis is carried out where each rotor blade is modeled individually such that rotor dissimilarity can be considered. A fuselage NASTRAN model is incorporated and coupled with the rotor model analysis. The centrifugally tuned, hub-mounted bifilar vibration absorbers are also modeled, and the coupled rotor-fuselage-bifilar nonlinear equations are solved using finite element method in space and time. Predicted 1/rev and 4/rev vibrations at pilot and copilot seats showed acceptable trends for magnitude and phase with flight-test data.

Nomenclature

C = modal damping matrix
D = diameter of the slot, in.
D_p = diameter of the tuning pin, in.
F = force vector
K = modal stiffness matrix
M = modal mass matrix
N_b = number of blades of a rotor
R = distance from pendulum rotation center to hub center of rotation, in.
r = radius of the pendulum arm, in.
w = blade-flap displacement
δT = variation of kinetic energy
δU = variation of strain energy
δW = virtual work
ξ = modal response
$\dot{\xi}$ = modal speed
$\ddot{\xi}$ = modal acceleration
ϕ = blade torsional deflection, deg.
ϕ_s = pitch-control rod bearing free-play, deg
ψ = azimuth angle
Ω = rotor rotation speed, rad/s
ω = natural frequency of vibration absorber, rad/s

Subscripts

a_i = ith vibration absorber
b_i = ith blade
f = fuselage
fa, af = absorber/fuselage coupling
fr, rf = rotor/fuselage coupling
r = rotor

Received 13 November 2001; revision received 1 May 2003; accepted for publication 20 June 2003.

*Graduate Research Assistant, Alfred Gessow Rotorcraft Center, Department of Aerospace Engineering. Student Member AIAA.
†Alfred Gessow Professor and Director, Alfred Gessow Rotorcraft Center, Department of Aerospace Engineering. Fellow AIAA.
‡Aerospace Engineer, Marine and Aviation Department, Carderock Division. Associate Fellow AIAA.

Introduction

A HELICOPTER rotor system operates in a highly dynamic and unsteady aerodynamic environment that can lead to severe vibratory loads. Over time, this can lead to wear in many rotor-system components such as bearings, dampers, and attachment fittings and results in high fuselage vibrations. In some cases high vibrations can be reduced by adjustments in the rotor-system track and balance through adjustment of trim tabs and control rods or by adding or removing balance weights. In other cases adjustments alone might not be effective, and a faulty component must be identified and replaced. This requires additional maintenance and might necessitate additional test flights and a highly trained expert to perform the diagnosis. These factors contribute to the high operating costs associated with helicopter rotor systems.

Flight critical components are designed using safe-life principles. Such configurations require conservative time-based component replacement intervals. When components in the rotor system are removed for maintenance, inspection or replacement, rotor track and balance must be checked and readjusted if necessary, adding further to the maintenance costs of rotor systems.

In an effort to reduce maintenance costs, health and usage monitoring systems typically incorporate onboard instrumentation to continuously monitor vibrations and rotor-blade response so as to carry out rotor track and balance adjustments in small increments between flight intervals. One concern with this approach is the possibility that faults or damage in the rotor system be "masked" by adjustments in rotor track and balance. Despite this concern, onboard rotor track and balance instrumentation offers a convenient basis to perform rotor-system health monitoring and fault detection when coupled with a suitable rotor system fault database. Unfortunately, flight-test data for rotor systems with prescribed faults are either unavailable or very limited because of safety of flight concerns. As a result, a mathematical model that can simulate rotor-system misadjustments, damage, and faults and can relate these conditions to fuselage vibrations and blade response will help provide the required seeded fault data needed to develop comprehensive fault diagnostic and prognostic algorithms.

Research on health and usage monitoring of helicopter rotor-system faults is limited. The theoretical basis of the rotor-system fault detection methodology is that for an ideal rotor all blades are

identical and the rotor acts as a filter with passage frequencies equal to multiple of N_b/rev. For example, for a four-bladed rotor, only 4, 8, 12, etc. per rev hub loads are transmitted to the fuselage. If there is a fault in one blade, that is, the blades are no longer identical, all of the harmonics will be transmitted through the hub resulting in higher fuselage vibrations. In addition, the response of the faulty blade will also be different from the others.

Ganguli et al.[1–4] developed a comprehensive aeroelastic model for studying the rotor response and hub loads for various rotor-system faults. Many types of faults were investigated including moisture absorption, loss of trim mass, damaged pitch-link, misadjusted tab, defective lag damper, free play in the pitch-control system and lag damper, friction in the flap and lag hinges and pitch-control system, blade structural damage, and chordwise mass imbalance. The faults were modeled by changes in blade inertia and structural and aerodynamic properties for the affected blade. A diagnostic table based on the system response in the presence of different rotor faults was developed. That research showed that most global faults, such as moisture absorption, loss of trim mass, misadjusted tab, and damaged pitch-link, etc., could be detected by monitoring rotor response and vibratory hub loads. However, localized faults such as blade cracks could not be detected by using global fault detection approach because the changes of system responses induced by localized faults are not significant enough to be detectable by standard rotor track and balance instrumentation. These studies incorporated an elastic rotor and a six-degree-of-freedom rigid fuselage model, but did not consider flexibility of the fuselage or rotor-fuselage couplings. In Ref. 4 a hybrid model based partly on physics and partly on flight-test data was used to develop a fault detection methodology. A neural-network approach was adopted to represent the relationship between hub loads and airframe vibration with faults. Flight-test data were used to train and test the neural network.

Azzam and colleagues[5–7] developed a mathematical model that was capable of predicting rotor-system fault-induced vibrations. Their model was used to provide the vibration data caused by a wide range of seeded faults for the development of advanced rotor-system fault diagnostics. In their mathematical model[5] the elastic rotor was assumed to undergo flapwise, lagwise, and torsional motions. Also, fuselage rigid-body motions were considered. Rotor-system faults were modeled by changing blade structural, aerodynamic, and inertia properties. This model was validated with some limited flight-test data for in-field vibrations induced by rotor adjustable faults.[6] The mathematical model generated a large database in order to train the neural networks in the development of artificial-Intelligence techniques for fault diagnostics and fatigue management. In Ref. 7 Wallace and Azzam developed a finite element model for the Lynx helicopter using MSC/NASTRAN. This model consisted of over 14,000 elements and was coupled with the rotor model used in Ref. 6 to relate the rotor hub loads to vibration and stresses at fuselage locations of interest.

Fuselage vibration is monitored and analyzed for rotor-system health monitoring. The vibration level must be kept below specified values in the system; otherwise, an adjustment or inspection is required to identify and correct the cause. The faults can be categorized into two groups: adjustable and nonadjustable faults. The adjustable faults are the ones that can be corrected by readjustment, such as mass imbalance, misadjusted pitch-control link, and trim-tab faults. The nonadjustable faults, such as pitch-control link free play, refer to component faults that require replacement. To make the proper adjustment or identify a fault, the relationship between the fault and corresponding airframe vibration must be known. Typically, for adjustable faults this relationship is determined experimentally by performing a series of flight tests to make all possible adjustments until a suitable mapping can be established. Ideally, the data set should contain combinations of various adjustments at several levels to capture nonlinear and coupling effects. This approach becomes more difficult for nonadjustable component faults (e.g., faulty bearings, dampers, etc.) because of safety of flight concerns.

The objective of this work is to develop a sufficiently detailed analytic model so that the effect of rotor-system faults on vibrations and blade response can be predicted. To accomplish this, a comprehensive rotorcraft analysis is needed that includes modeling of fuselage structural details and rotor-fuselage dynamic coupling.

Even though a great deal of effort by researchers has been devoted to improving the analysis and mathematical modeling of rotor-fuselage systems, reliable and accurate vibration prediction is still a challenging problem. The state of the art in the prediction of rotor loads is less than satisfactory. In Ref. 8 the vibratory hub loads predictions from eight advanced aeroelastic codes were correlated with Lynx flight-test measurements at both low (64 kns) and high (158 kns) flight conditions. First, a baseline model for each code with same characteristics was established to quantify the improvement necessary to upgrade to current technology standard. The effects of various analytical modeling techniques, such as free wakes, fuselage upwash, unsteady aerodynamics and complete finite element representation vs modal approximation, on the vibration correlation, in terms of both magnitude and phase, were examined. All of these codes showed considerable errors in predicting rotor loads. On average, codes were unable to predict vibratory loads to an accuracy greater than 50% of the Lynx measurements, and no single code outperformed others for all load components and flight conditions.

Most comprehensive analyses are restrictive in terms of modeling airframe vibrations and typically assume an ideal rotor with similar blades. A few selected coupled rotor/fuselage analyses consider flexibility of both rotor and fuselage in a consistent manner. Recently, Yeo and Chopra[9,10] developed a comprehensive coupled rotor/fuselage vibration analysis and incorporated it into UMARC (University of Maryland Advanced Rotorcraft Code). The authors correlated their calculated results with AH-1G flight-test data. Their studies showed that significant differences exist in the predicted vibration level using a rigid fuselage as compared to using an elastic fuselage model. To predict fuselage vibration accurately, a refined fuselage model is essential, and a free-wake model must also be included. However, their analysis assumed that the blades were identical. With the presence of faults, this assumption is no longer valid.

For present study the UMARC that was upgraded by Yeo and Chopra[9,10] has been reformulated to account for a dissimilar rotor. An analytic model that couples a nonideal, dissimilar rotor system with hub-mounted vibration absorbers to a fully elastic three-dimensional fuselage model is utilized. The finite element method in space and time is used to solve the coupled rotor-fuselage system. Dissimilarity among rotor blades as well as dynamic coupling among rotor, fuselage and vibration absorbers are considered in a consistent manner. Airfoil and fuselage aerodynamic data tables are used to determine nonlinear aerodynamic loads. A pseudo-implicit free-wake model developed by Bagai and Leishman[11] is adopted to calculate the inflow distribution in the rotor. The analysis is carried out using rotor properties similar to an SH-60 helicopter with selected rotor track and balance misadjustments and component faults. Airframe vibration and blade track results under different faults and different airspeeds are presented and compared with flight-test data.

Formulation

The formulation consists of two parts: modeling the helicopter system and modeling of the rotor-system faults.

System Governing Equations

The helicopter system consists of three parts: a rotor with elastic blades, elastic fuselage, and hub-mounted vibration absorbers. These parts are coupled through the rotor hub. Blades are modeled individually such that rotor-system faults can be simulated. Each blade undergoes flap bending, lag bending, elastic twist, and axial deformation. Each bifilar absorber has one degree of freedom and is coupled with hub in-plane motion. The fuselage is considered elastic, and the hub is set free in the air, that is, it undergoes six-degrees-of-freedom motions (three translational and three rotational).

The formulation of the completed system is based on Hamilton's principle for a nonconservative system[12]

$$\int_{t_1}^{t_2} (\delta U - \delta T - \delta W)\, \mathrm{d}t = 0 \tag{1}$$

where the δU, δT, and δW are the variations of the system strain energy, kinetic energy, and the virtual work done by external forces, respectively. The energy variation consists of contributions from each blade, absorber, and the fuselage:

$$\delta U = \sum_{i=1}^{N_b} \left(\delta U_{b_i} + \delta U_{a_i}\right) + \delta U_f \tag{2}$$

$$\delta T = \sum_{i=1}^{N_b} \left(\delta T_{b_i} + \delta T_{a_i}\right) + \delta T_f \tag{3}$$

$$\delta W = \sum_{i=1}^{N_b} \left(\delta W_{b_i} + \delta W_{a_i}\right) + \delta W_f \tag{4}$$

Because the fuselage motion is expressed in the nonrotating system, the rotor equations and absorber equations are transformed into the fixed system by using the Fourier coordinate transformation. The finite element method is used to model blade and fuselage structures. For computational efficiency the governing equations are transformed into modal space. The modal equations of the dynamically coupled system can be expressed symbolically as

$$\begin{bmatrix} M_{\mathrm{rr}} & M_{\mathrm{rf}} & 0 \\ M_{\mathrm{fr}} & M_{\mathrm{ff}} & M_{\mathrm{fa}} \\ 0 & M_{\mathrm{af}} & M_{\mathrm{aa}} \end{bmatrix} \begin{Bmatrix} \ddot{\xi}_r \\ \ddot{\xi}_f \\ \ddot{\xi}_a \end{Bmatrix} + \begin{bmatrix} C_{\mathrm{rr}} & C_{\mathrm{rf}} & 0 \\ C_{\mathrm{fr}} & C_{\mathrm{ff}} & C_{\mathrm{fa}} \\ 0 & C_{\mathrm{af}} & C_{\mathrm{aa}} \end{bmatrix} \begin{Bmatrix} \dot{\xi}_r \\ \dot{\xi}_f \\ \dot{\xi}_a \end{Bmatrix}$$

$$+ \begin{bmatrix} K_{\mathrm{rr}} & K_{\mathrm{rf}} & 0 \\ K_{\mathrm{fr}} & K_{\mathrm{ff}} & K_{\mathrm{fa}} \\ 0 & K_{\mathrm{af}} & K_{\mathrm{aa}} \end{bmatrix} \begin{Bmatrix} \xi_r \\ \xi_f \\ \xi_a \end{Bmatrix} = \begin{Bmatrix} F_r \\ F_f \\ 0 \end{Bmatrix} \tag{5}$$

The formulation incorporates consistent structural, aerodynamic, and inertial coupling effects among rotor, absorbers, and fuselage.

Having obtained the blade and fuselage response, hub loads are calculated using the force summation method to solve the vehicle equilibrium equations. For steady flight the vector summation of all of the steady forces and moments applied on the vehicle should be balanced, that is, $\sum \boldsymbol{F} = 0$ and $\sum \boldsymbol{M} = 0$. To accurately represent the aerodynamic forces, airfoil and fuselage aerodynamic characteristics in terms of table look-up are used. A pseudo-implicit free-wake model[11] is used to model the inflow distribution in the rotor. A coupled trim procedure is used to solve the system responses and vehicle equilibrium equations simultaneously. The iteration terminates when the solution to the rotor/fuselage/absorber responses and vehicle equilibrium equations converges.

Bifilar Absorber

Vibration absorbers are commonly installed on helicopters. Some of them are mounted on the airframe and are normally considered in the fuselage modeling. Others are mounted on the hub and should be included in the rotor modeling. The bifilar vibration absorbers system (Fig. 1) is a vibration suppression device centrifugally tuned to cancel vibratory loads at certain frequency. The bifilar undergoes in-plane motion. For a four-bladed rotor the sources of the 4/rev in-plane loads in the nonrotating system are 3/rev and 5/rev chordwise shears in the rotating system. The absorbers are tuned to cancel these loads at the rotating system such that 4/rev nonrotating frame loads can be reduced. By reducing the 4/rev excitation forces the fuselage 4/rev vibration level will be reduced.

From Refs. 13 and 14 the bifilar absorber can be simplified as a simple pendulum attached to the hub (Fig. 2a). By using the small angle assumption, the pendulum's natural frequency ω equals $\Omega\sqrt{(R/r)}$. When ω equals the excitation frequency, the pendulum acts as a vibration absorber. When Ω is known, the natural frequency of the pendulum can be adjusted by setting the ratio of R/r. For example, in order to achieve a natural frequency of 4Ω the R/r ratio has to be 16. However, for the helicopter rotor hub the size of R is limited, and the pendulum arm r has to be very small to meet the requirement. The bifilar absorber is used to solve this problem. As illustrated in Fig. 2b, the natural frequency of the bifilar is

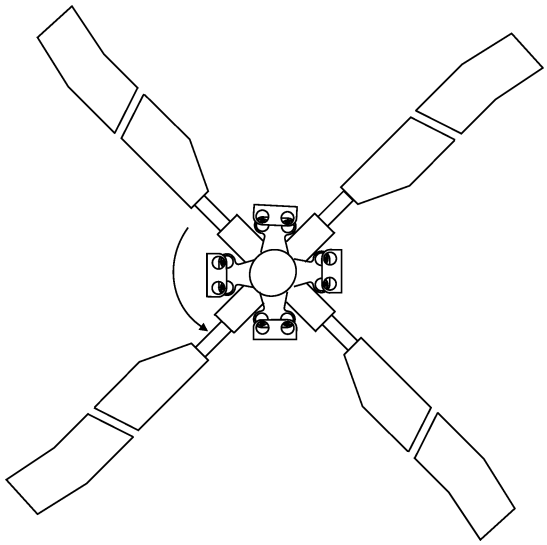

Fig. 1 H-60 rotor bifilar installation.

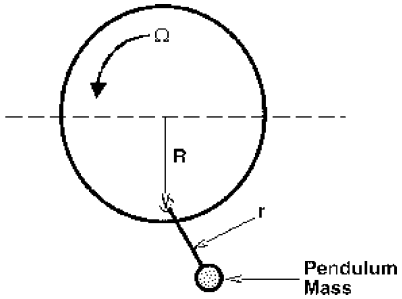

a) Simple Pendulum

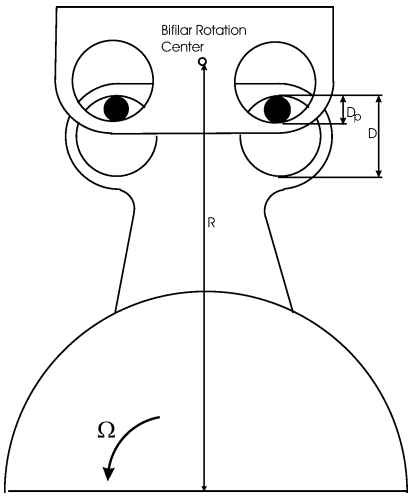

b) Bifilar

Fig. 2 Simple pendulum and bifilar.

$\omega = \Omega\sqrt{[R/(D - D_p)]}$. By adjusting the diameter of the tuning pin D_p close to the diameter of the slot D, the bifilar can have desired natural frequency.

Rotor-System Fault Modeling

The faults that are examined in this paper are referred to as global faults. The word global comes from the fact that these faults cause measurable changes in global system parameters such as airframe vibrations and blade-tip flap and lead-lag deviations. They are distinguished from nonglobal faults, such as blade local structural cracks. These faults are modeled as changes in blade properties from baseline values. The finite element method allows for

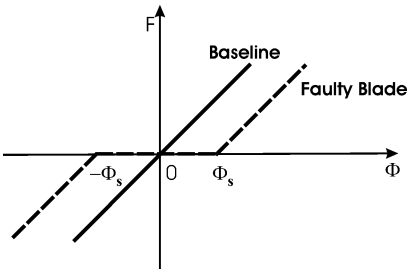

Fig. 3 Pitch-link load for blade with pitch-link free play.

a detailed discretization of blade structural properties and boundary conditions. It also provides the means to model various faults through changes in blade inertial, stiffness, damping, or aerodynamic characteristics. Each blade is modeled individually to allow for dissimilarities from others. The following list describes the faults examined in this study and describes how they are modeled.

1) Mass imbalance is the first fault. For this fault the mass distribution of the faulty blade is different from that of others. It is modeled by changing the appropriate blade mass distribution. During the rotor track and balance operation, balancing weights can be added to or removed from a specified blade station located close to the root.

2) Misadjusted pitch-control link is the second fault. The faulty blade has a different pitch setting from that of others, causing an aerodynamic dissimilarity.

3) The misadjusted trim-tab fault is represented by having the trim-tab on one blade bent up or down at a different height relative to the others. The trim-tab can be viewed as a flap. The bent-up or-down adjustments resulted in changes of the airfoil aerodynamic properties. Based on Ref. 15, this fault is modeled by changing the blade sectional zero-lift angle and aerodynamic pitch moment within the tab region.

4) Pitch-control bearing free play is the last fault. Because of wear and tear of the bearing, the pitch-link can have some free play, that is, when the blade torsional deformation at the pitch link is less than the free-play angle ϕ_s, the pitch-link load is zero. This fault is modeled by expressing the pitch-link load in a nonlinear manner (Fig. 3):

$$F = \begin{cases} 0 & \text{for} \quad |\phi| < \phi_s \\ K_\phi(\phi - \phi_s) & \text{for} \quad \phi \geq \phi_s \\ K_\phi(\phi + \phi_s) & \text{for} \quad \phi \leq -\phi_s \end{cases} \tag{6}$$

The faults just mentioned can be categorized into two groups: adjustable and nonadjustable faults. The adjustable faults include mass imbalance, misadjusted pitch-control link, and trim-tab faults. The nonadjustable fault includes pitch-control link free play.

Results and Discussion

A four-bladed articulated rotor similar to the SH-60 aircraft and a detailed NASTRAN finite element model of the SH-60 fuselage that has more than 8400 elements are used for the results. Table 1 shows the basic parameters of the helicopter. Based on the convergence study, each blade is discretized into 12 beam elements (with each element undergoing flap, lag, torsional and axial motions), and the modal equations of each blade are based on eight coupled modes. Four identical bifilar absorbers are attached to the rotor hub with a natural frequency of 3/rev to absorb the 3/rev blade in-plane shears in the rotating system. Figure 4 shows the SH-60 fuselage finite element model that was developed by Sikorsky. In the analysis MSC NASTRAN is used to calculate fuselage mode shapes, modal mass, and natural frequencies. These data are used as inputs for the coupled rotor-fuselage analysis. Based on the convergence study, 34 fuselage modes (six rigid, 28 elastic modes) are used in this analysis. Predicted fuselage frequencies using NASTRAN are compared with the available shake-test data. Results show that most of the predicted frequencies are within about 10–20% of the measured shake-test results (Fig. 5). It should be kept in mind that the NASTRAN model might not be a true representation of the shake-test airframe.

Table 1 Baseline helicopter properties

Property	Value
Gross weight	19,000 lb
Center-of-gravity location	Below the shaft
Rotor radius	26.8 ft
Number of blades	4
Rotor-tip speed	725 ft/s
Blade chord	20.76 in.
Flap and lag hinge offset	15 in.
Blade linear twist	−18 deg
Airfoil type	SC1095 SC1095RC
Lock number	8
Solidity	0.0826

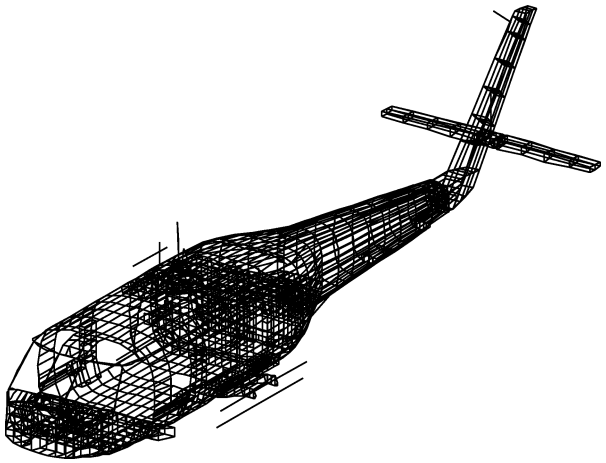

Fig. 4 SH-60 fuselage NASTRAN model (developed by Sikorsky).

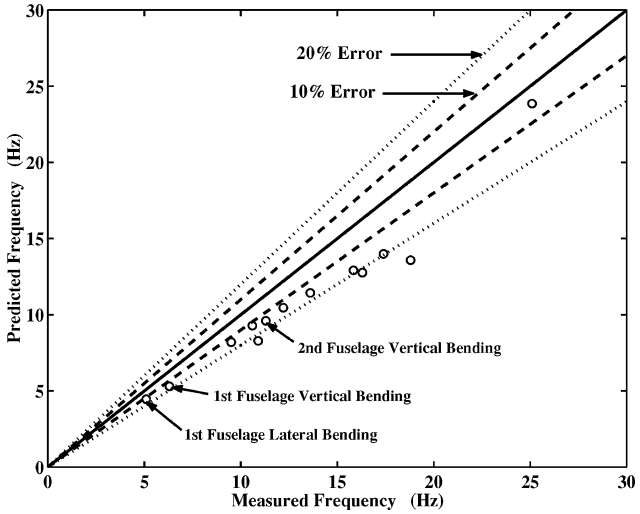

Fig. 5 SH-60 fuselage frequency diagram.

Selected rotor-system faults are simulated and compared with available flight-test data collected during the Air Vehicle Diagnostic System Program.[16] An SH-60F aircraft was used to collect data for both baseline (no prescribed fault) and faulted configurations. Because the location of the aircraft center of gravity was not recorded during the flight test, it is assumed beneath the rotor shaft for present calculation. Figure 6 shows a schematic view of the blade with absorbers. Blade one locates at the zero azimuth angle. For each prescribed fault configuration three flights were performed. First, a baseline flight (no fault, 1/rev vibration within limit) was flown. Then a faulty component or misadjustment was added, and the aircraft flew again. After the faulty component was removed or the

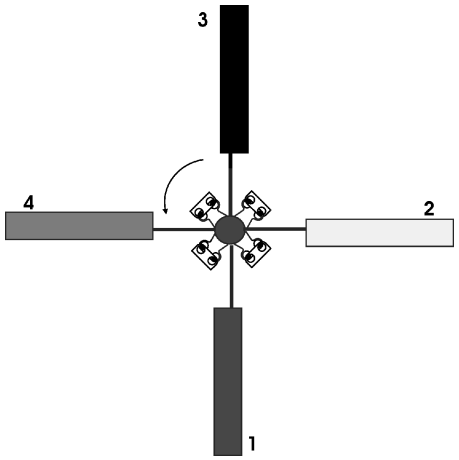

Fig. 6 Rotor-blade index.

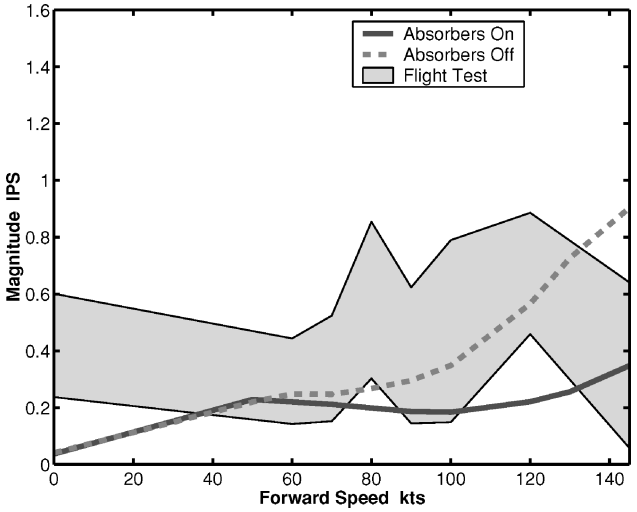

Fig. 7 Baseline 4/rev vibration at A (copilot).

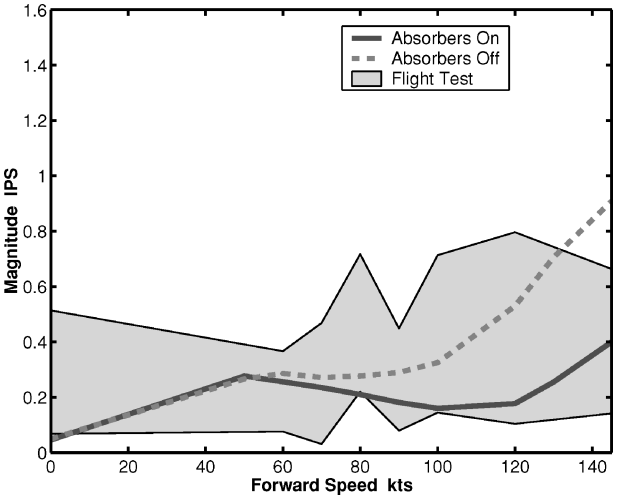

Fig. 8 Baseline 4/rev vibration at B (pilot).

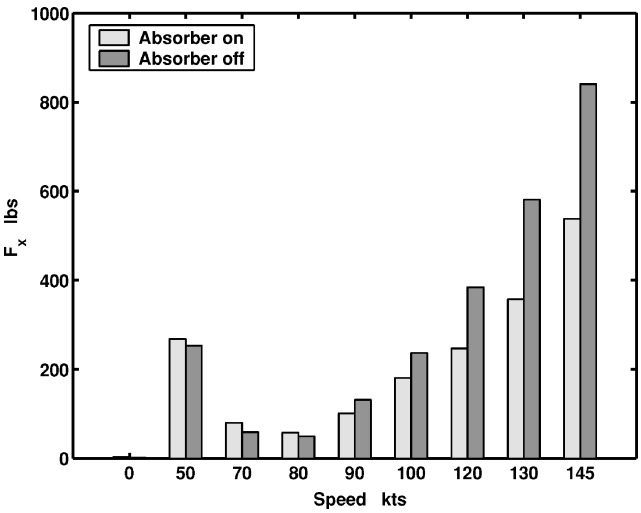

Fig. 9 Baseline 4P longitudinal hub force.

misadjustment was corrected, another flight was conducted to ensure that the aircraft was returned to baseline condition again. During the flight test, airframe vertical vibration signals (both magnitude and phase) were recorded at the copilot (station A) and pilot (station B) seats bulkhead for each flight condition. Data were collected in steady level flight from hover to 145 kn. The measured vibration data are expressed in terms of velocity (inches per second). During the flight test, an optical tracker was mounted on the aircraft nose (azimuth angle 180 deg) to measure the blade flap and lead-lag displacements.

Baseline Results

The baseline configuration refers to a helicopter without any fault in the rotor system. In the numerical simulation the baseline configuration is an ideal rotor with four identical blades. For such a system only multiples of N_b/rev vibratory loads are transmitted to the fuselage during forward flight causing primarily N_b/rev vibration. However, for a real rotor there are always some dissimilarities between rotor blades because of manufacturing or assembly differences or component wear. Therefore, the flight vehicle experiences vibration at all harmonics in hover and forward flight, even for the baseline configuration. A rotor can be considered as a baseline when its fuselage 1/rev vibration is lower than a certain tolerable value.

Figures 7 and 8 compare the 4/rev vibration magnitude at station A (copilot) and station B (pilot) between flight test and prediction. Because the flight-test data represent several sets of baseline data collected over the span of the flight-test program, there is significant scatter in the data. The prediction shows that at low speeds wake causes high vibration. As speed increases, wake effect decreases, and the vibration decreases. As speed goes higher, vibration increases again because of nonlinear aerodynamic loads. Analysis shows that vibration absorbers are very effective in reducing vibration in forward flight (above 60 kn). They not only reduce the magnitude of vibration at certain flight speeds, but also keep the vibration increment with flight speed smaller. The explanation for this is that the absorbers reduce the 4/rev in-plane hub loads that contribute to the vibration. Figures 9 and 10 show the baseline 4/rev longitudinal and lateral hub forces respectively with and without absorbers. Longitudinal hub force is reduced significantly at high speed while the lateral force has little change. The analysis shows the importance of including proper hub modeling in the vibration prediction.

Rotor-Fault Cases

When there is a fault in the rotor system, the rotor no longer acts like an ideal filter; all of the harmonics of loads will be transmitted to the fuselage. This generally increases airframe vibration. For the rotor health monitoring the 1/rev vibration and blade track height are monitored as indicators of the condition of the rotor.

Flight tests for the baseline case (no fault) show 1/rev vibration indicating the inherent dissimilarity in the rotor. When a fault is added, the measured 1/rev vibration includes the contribution from the inherent dissimilarity in the baseline plus the contribution from the added fault. The change (in a vector sense) of the 1/rev vibration is introduced by the fault. In the analytical model the baseline does not have any 1/rev vibration because each blade is assumed identical.

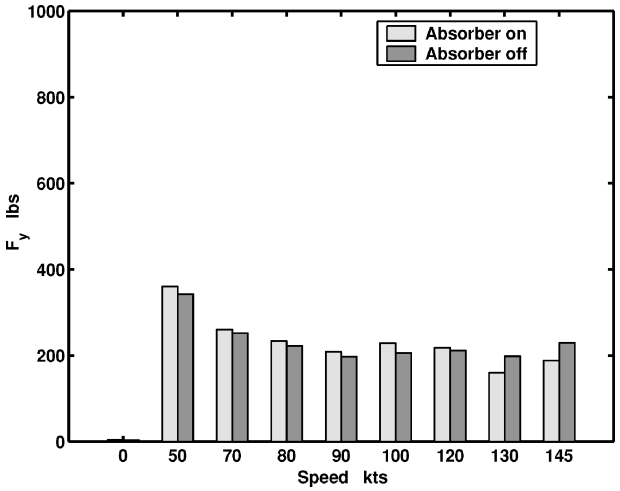

Fig. 10 Baseline 4P lateral hub force.

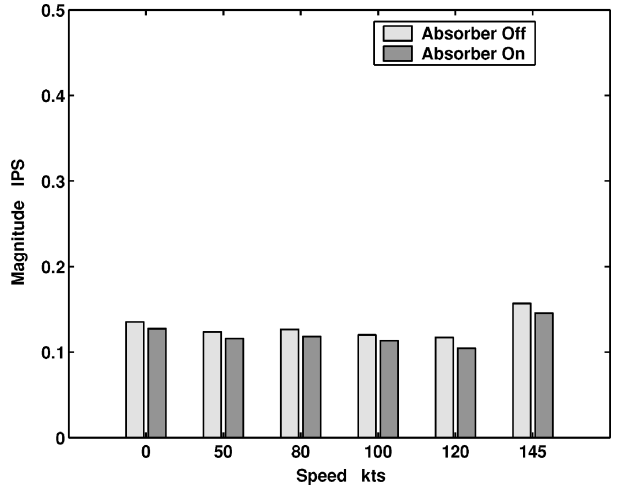

a) Imbalanced Mass Fault

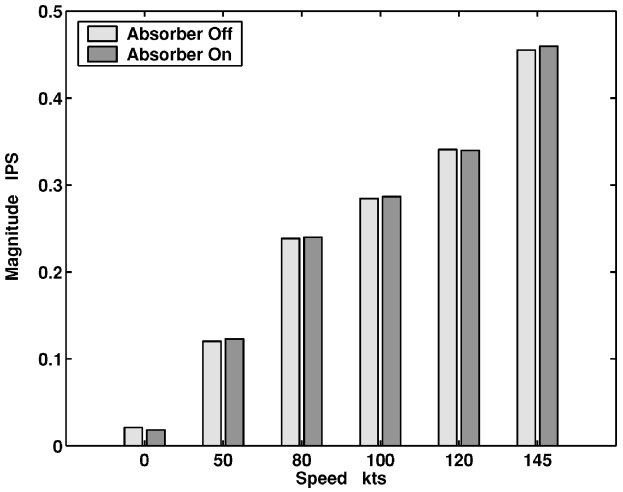

b) Trim-Tab Fault

Fig. 11 1P pilot seat vibration caused by rotor-system faults.

The 1/rev vibration is introduced solely by the fault. For comparison purposes all results are given in terms of the differences between the baseline and fault configurations.

Effect of Absorbers

It was shown before that vibration absorbers reduce 4/rev vibration significantly. The effect of vibration absorbers on the 1/rev fuselage vibration caused by a rotor system fault is also of interest.

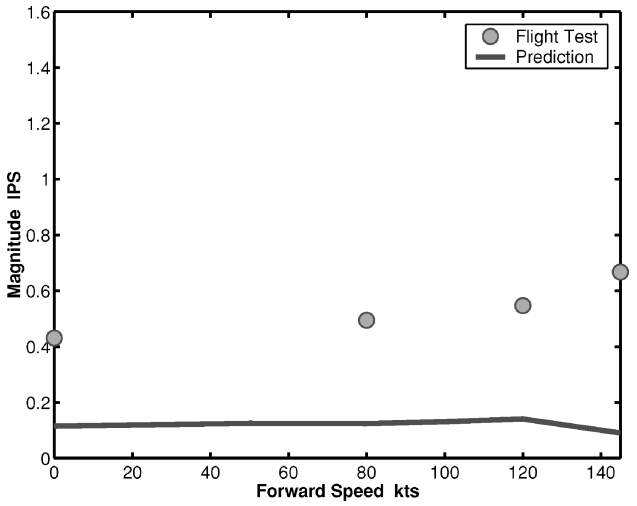

a) Magnitude

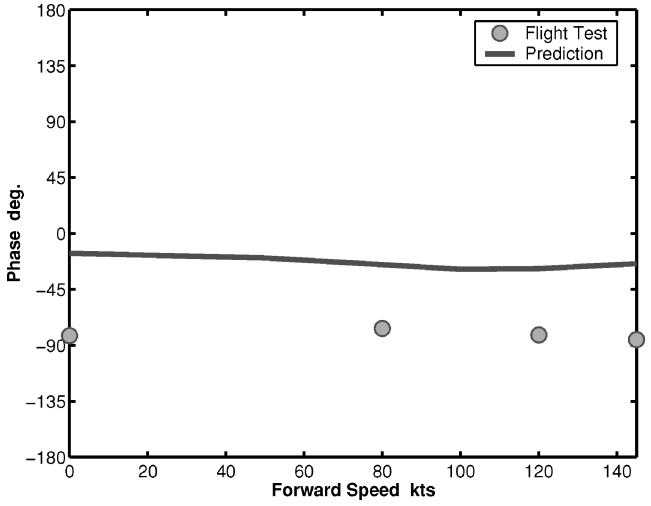

b) Phase

Fig. 12 Change in 1/rev vibration at station A (copilot) as a result of mass imbalance fault.

Figure 11a shows the predicted 1/rev vibration at the pilot seat as a result of an imbalanced mass fault. Two adjacent blades, blade 1 and 2, had weight increases of 5 lbs and 4.5 lbs respectively. The analysis shows a very small change in the 1/rev vibration between absorber enabled cases and absorber disabled cases.

Figure 11b shows the 1/rev vibration at the pilot seat as a result of a trim-tab fault. The trim-tab of blade 2 was bent down 0.02 in. from the baseline position. Again, the analysis shows a very small difference in the vibration level between absorber enabled and disabled cases.

Because the absorbers are tuned to absorb the 4/rev harmonic in the nonrotating system, they have a small effect on the 1/rev harmonic because of the rotor dissimilarity.

Imbalanced Mass Fault

For the SH-60 rotor balancing weights can be added or removed from a location close to the blade root to balance the rotor (41.5 in. from the shaft rotation center). During the flight test, a 5-lb weight was added to that location in blade 2, and a 3-lb weight was removed from that location in blade 4 to simulate an imbalanced rotor. This fault is modeled as a local mass change, and the blade elemental mass at that location is modified to reflect the change.

Figures 12 and 13 show the magnitude and phase of the 1/rev vibration at copilot(A) and pilot(B) seats. The predictions show that the vibration amplitude and phase do not vary much with flight speed because the vibration is mainly induced by centrifugal force, which

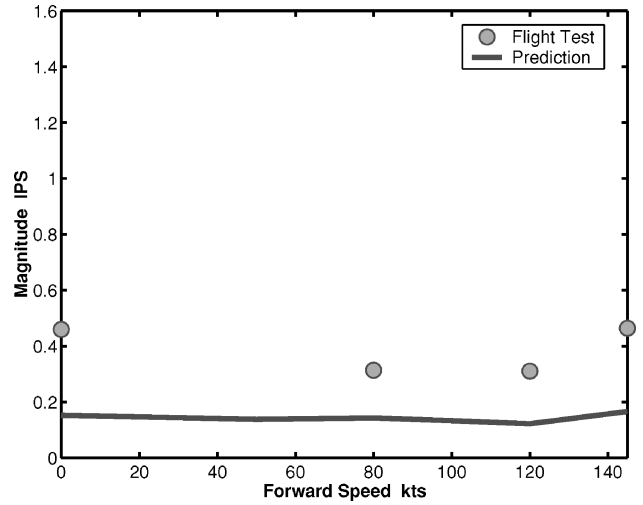

a) Magnitude

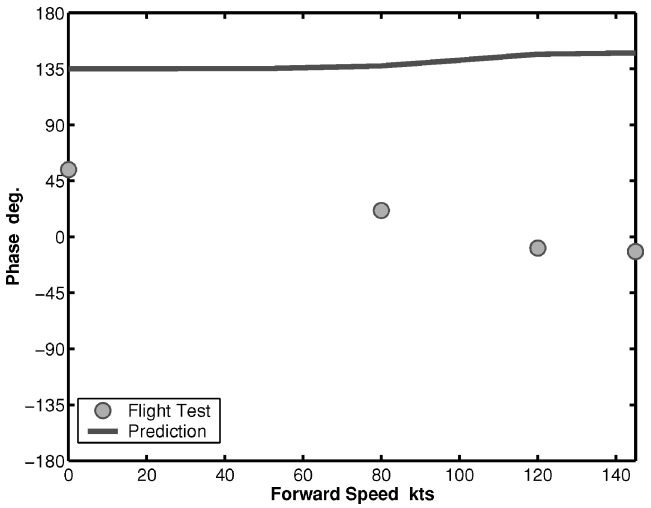

b) Phase

Fig. 13 Change in 1/rev vibration at station B (pilot) as a result of mass imbalance fault.

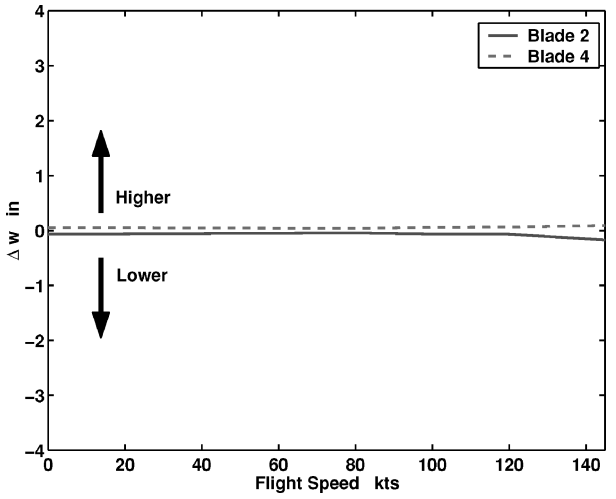

a) Flap

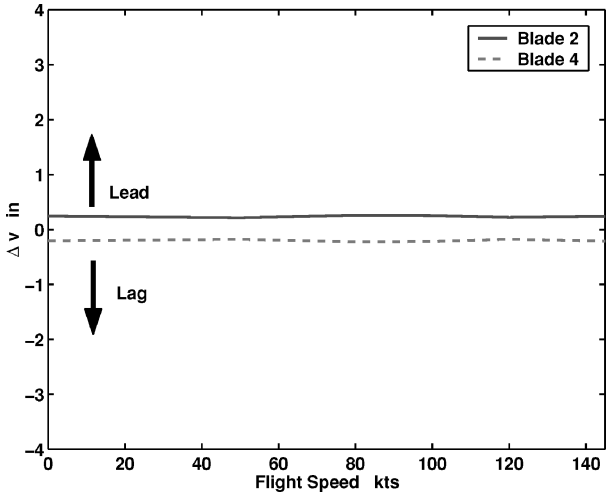

b) Lead-Lag

Fig. 14 Faulty blade-tip displacement deviation at 180-deg azimuth angle caused by mass imbalance fault.

is a function of rotor speed. The analytical results show a similar trend of phase variation with the test data at station A. In both cases the levels of vibration are underpredicted. Keeping in view the state of the art in the prediction of vibratory loads (less than 50%; see Ref. 8), this correlation of vibration level with flight-test data appears acceptable for the purpose at hand.

For a rotor with identical blades, each blade tip travels the same path. However, for a dissimilar rotor the tip path of the faulty blade can vary from the others. In the current study the blade-tip flap deviation is defined as

$$\Delta w_i(\psi) = w_i(\psi) - \bar{w}(\psi)$$

$$\bar{w}(\psi) = \frac{1}{N_b}\sum_{i=1}^{N_b}\left[w_1(\psi) + \cdots + w_{N_b}(\psi)\right] \tag{7}$$

where $w_i(\psi)$ is the ith blade-tip flap displacement at azimuth ψ and $\bar{w}(\psi)$ is the mean position of all of the blades. For the lead-lag displacement a similar definition applies.

Figure 14 shows the blade-tip flap and lead-lag deviations at 180-deg azimuth angle (aircraft nose) caused by the mass imbalance fault. (Test data are not available.) Results show that blade 2 flaps lower and blade 4 flaps higher than the mean position at 180° azimuth. Results also show that blade 2 leads and blade 4 lags the mean position. An important observation of the tip deviation caused by the mass fault is that the blade-tip displacement deviations are small and insensitive to the change of the flight speed.

Trim-Tab Fault

The trim-tab is a device used to track the rotor through a change in blade sectional aerodynamic properties. For the SH-60 helicopter the trim-tab extends the blade chord by 7% and spans from 70 to 87% of the blade radius. In the flight test blade 4 had its trim-tab bent up by 0.015 in. When deflected up, the trim-tab reduces blade sectional lift and introduces a nose-up pitch moment. Using experimental curves from Ref. 15, the change in trim-tab height can be related to the change in zero-lift angle and pitch moment at quarter-chord. In this study the effect of this misadjustment is equivalent to a decrease in zero-lift angle by 0.11 deg and an additional nose-up pitch-moment coefficient equal to 0.0042.

Figure 15 shows the magnitude and phase of the 1/rev vibration at copilot (A) seat as a result of the trim-tab fault. The prediction shows that the vibration magnitude increases with speed because change in trim-tab deflection affects sectional aerodynamic properties. The prediction also shows that the phase of vibration changes little with flight. The prediction captured the trend of the test data.

Figure 16 shows the vibration magnitude and phase of the 1/rev vibration at pilot (B) seat. Again, the magnitude of 1/rev vibration increases with flight speed. The phase has little change at forward flight except for the phase change from hover to forward flight. Flight-test data show the same trend.

Figures 17 shows the calculated blade-tip deviation caused by the trim-tab fault at the 180-deg azimuth angle. The faulty blade flaps higher than the mean position. The flap deviation caused by

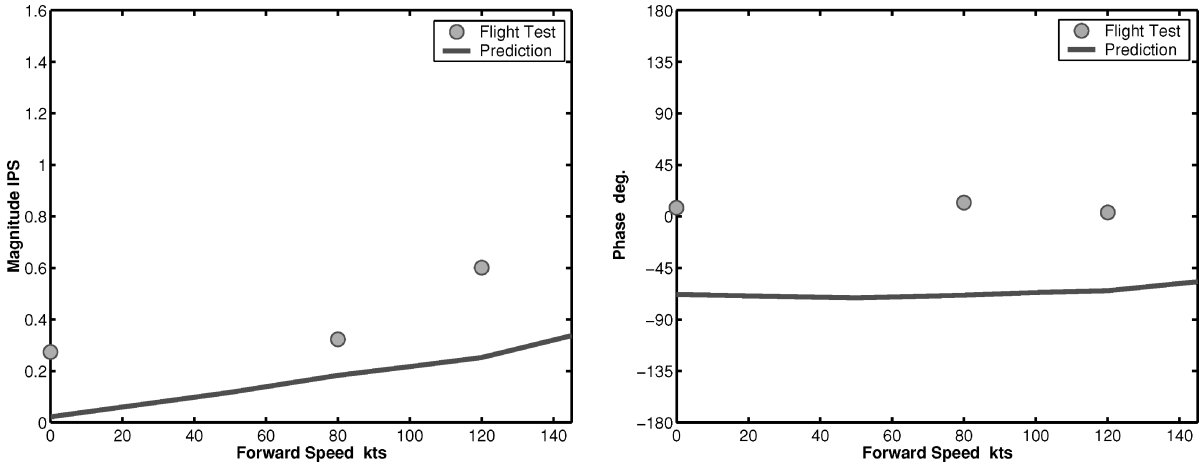

a) Magnitude b) Phase

Fig. 15 Change in 1/rev vibration at station A (copilot) caused by trim-tab 0.015 in. up.

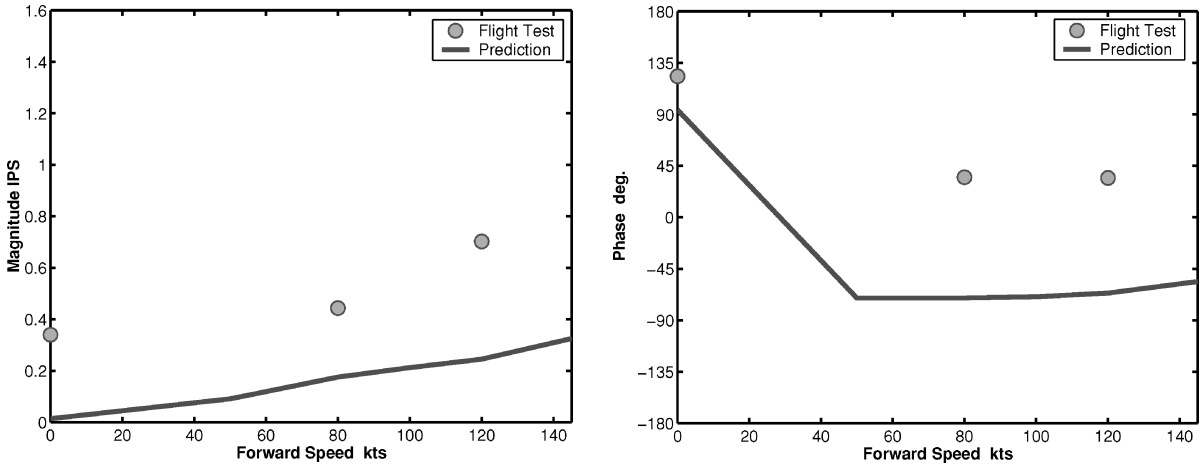

a) Magnitude b) Phase

Fig. 16 Change in 1/rev vibration at station B (pilot) caused by trim-tab 0.015 in. up.

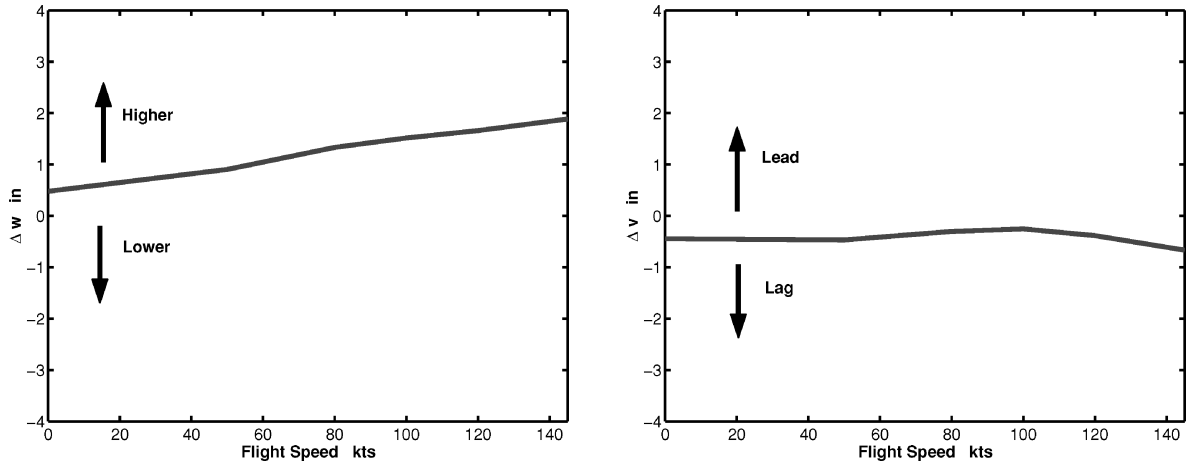

a) Flap b) Lead-Lag

Fig. 17 Faulty blade-tip displacement deviation at 180-deg azimuth angle caused by trim-tab 0.015 in. up.

this fault is about 0.5 in. at hover and increases to 1.9 in. as flight speed reaches 145 kn. Figure 17b shows that the faulty blade lags other blades. It also shows that the tip lead-lag deviation has little variation with flight speed.

Misadjusted Pitch-Control Link

During the flight test, pitch-link of blade one was adjusted 11 clicks down compared to the baseline configuration. From the hub geometric data this change is approximated by a 0.43-deg decrease in the pitch setting θ_0 for that blade. Thus the faulty blade has different aerodynamic loads than the others.

Figures 18 and 19 show the 1/rev vibration magnitude and phase at copilot (A) and pilot (B) seats, respectively. The prediction shows that the magnitude of the 1/rev vibration increases from hover to 80 kn and then gradually decreases as speed increases. In this case the prediction did not capture the flight-test data.

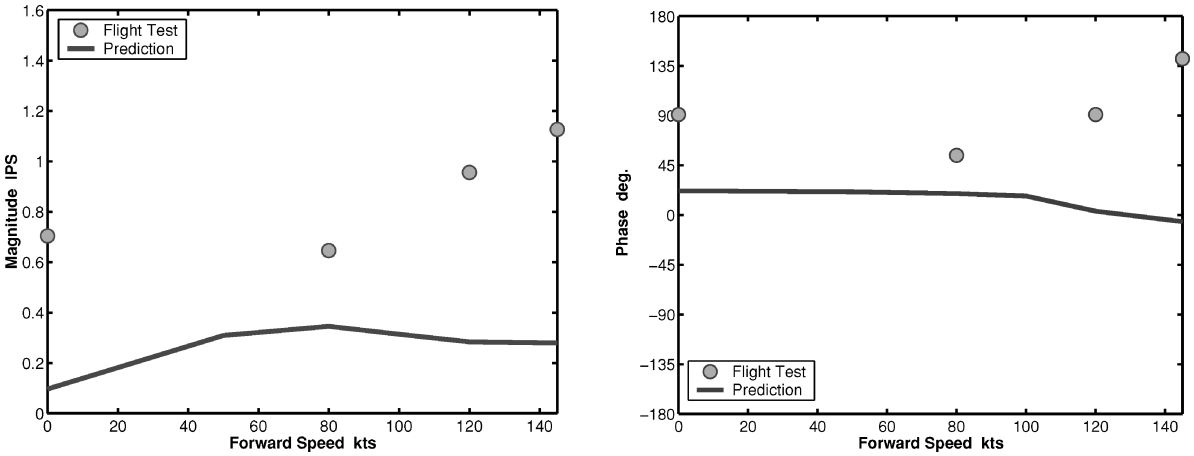

a) Magnitude b) Phase

Fig. 18 Change in 1/rev vibration at station A (copilot) caused by pitch-control link down 11 clicks.

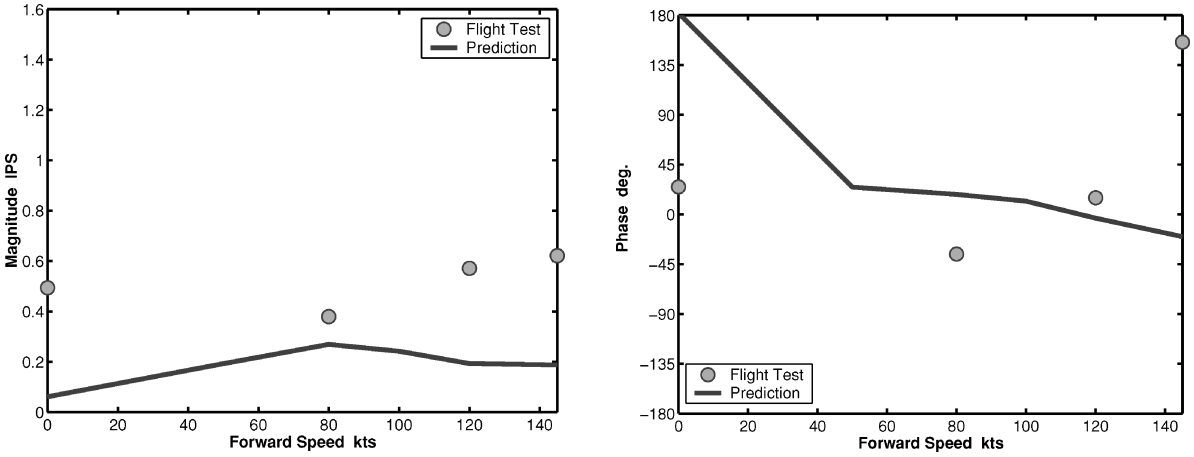

a) Magnitude b) Phase

Fig. 19 Change in 1/rev vibration at station B (pilot) caused by pitch-control link down 11 clicks.

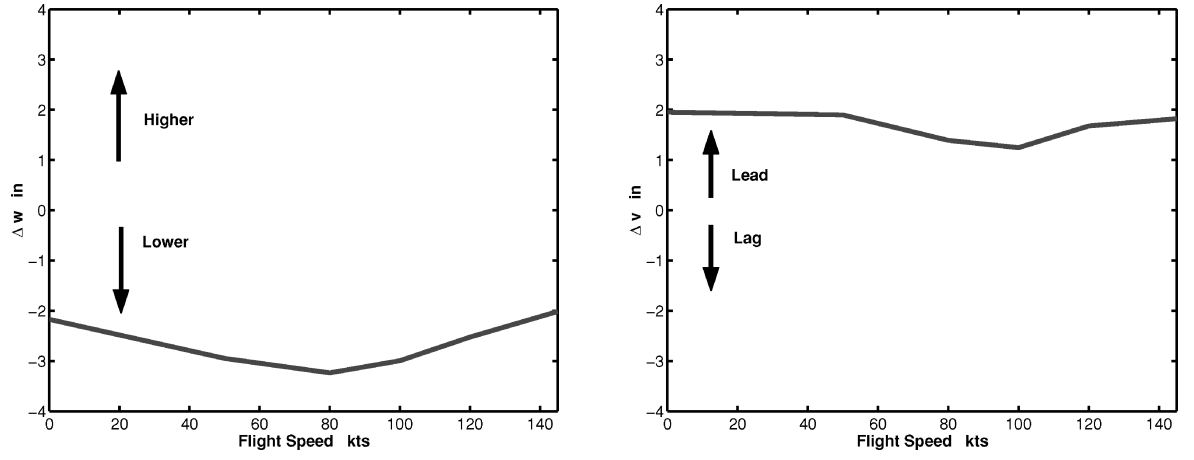

a) Flap b) Lead-Lag

Fig. 20 Faulty blade-tip displacement deviation at 180-deg azimuth angle caused by pitch-control link down 11 clicks.

Figure 20a shows the calculated flap deviation at the blade tip as a result of the pitch-control link misadjustment at 180-deg azimuth angle (aircraft nose). The blade flap height for the faulted blade is smaller than the other blades because it has a smaller collective pitch angle. As airspeed increases, the deviation increases from 2.1 in. at hover to 3.1 in. at 80 kn, then drops to 2 in at 145 kn.

Figure 20b shows the deviation of blade-tip lead-lag deflection between the faulty blade and the others at the 180-deg azimuth angle. The faulty blade leads other blades because it has smaller collective pitch, which generates less induced drag (because of reduced lift) and less profile drag (because of reduced angle of attack). As flight speed increases from hover to 100 kn, the amount of blade one leads the other blade decreases from 2 to 1.1 in., then it increases to 1.85 in. as speed increases to 145 kn.

Pitch-Control Link Free Play

The pitch-control system is subjected to vibratory blade loads, and over time the bearings can become worn causing freeplay. During

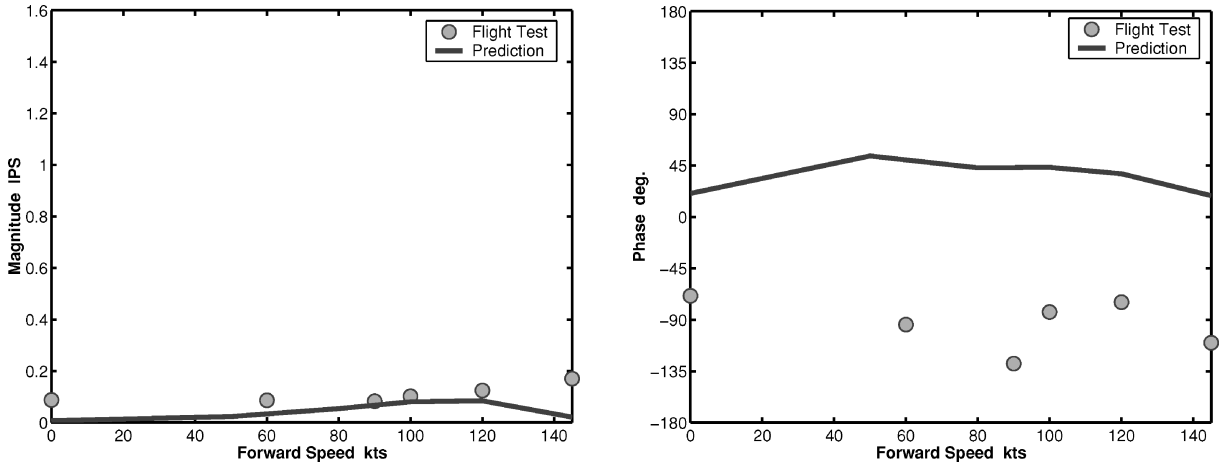

a) Magnitude b) Phase

Fig. 21 Change in 1/rev vibration at station A (copilot) caused by pitch-control link free play.

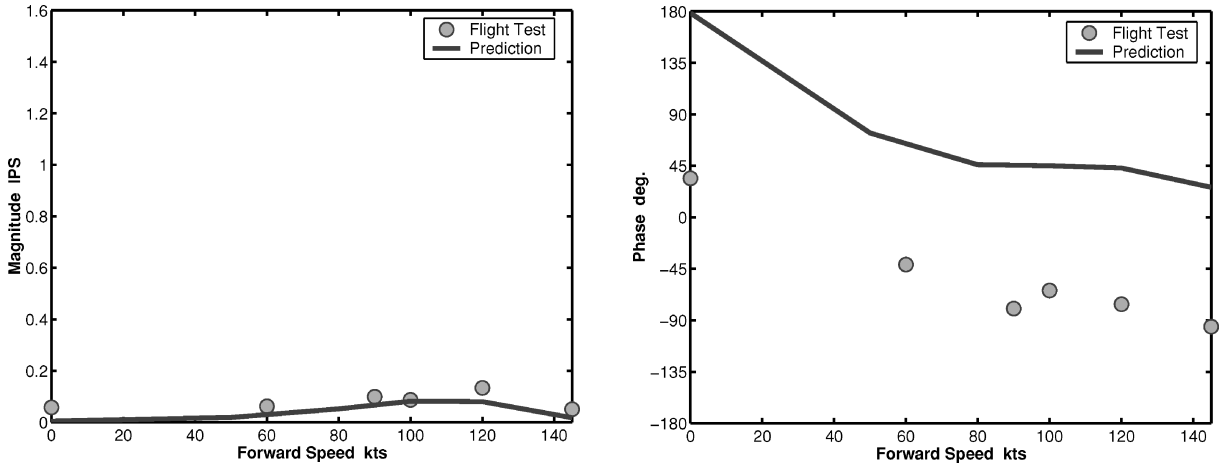

a) Magnitude b) Phase

Fig. 22 Change in 1/rev vibration at station B (pilot) caused by pitch-control link free play.

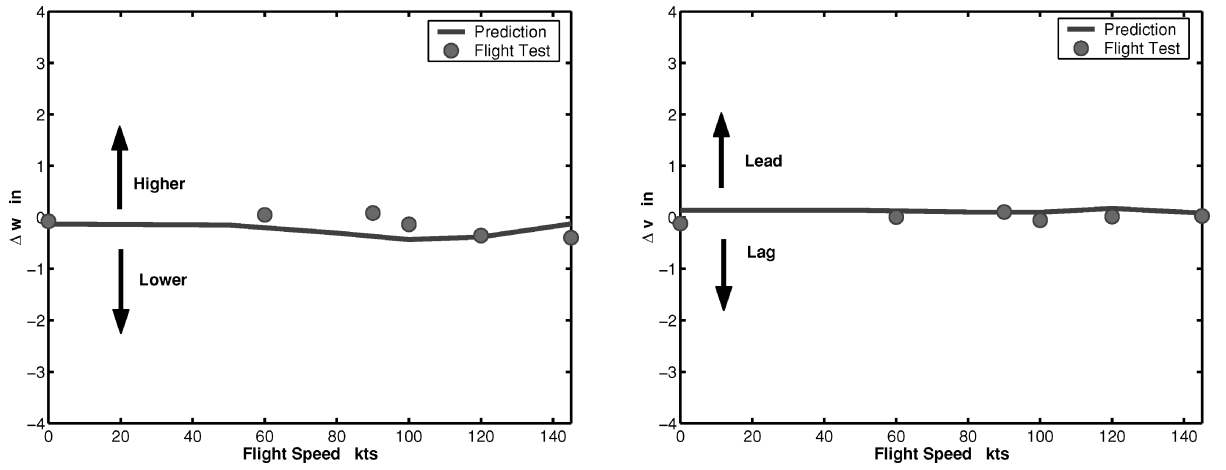

a) Flap b) Lead-Lag

Fig. 23 Faulty blade-tip displacement deviation at 180-deg azimuth angle caused by pitch-control link free play.

the flight test, a worn bearing with 0.015-in. clearance was installed in blade number one. Only when the blade torsion displacement exceeds the bearing free-play angle ϕ_s can the pitch-link take effect. Because of flight safety concerns, this fault level is still within the acceptable range for the bearing.

Figure 21 shows the vibration magnitude and phase at copilot seat (A). The prediction shows that the vibration magnitude increases with speed, except for a drop at 145 kn (Fig. 21a). The phase of the vibration does not vary much with airspeed (Fig. 21b). The prediction generally captured measured data for magnitude, except at 145 kn. And it also captures the trend of the phase.

Figure 22 shows the magnitude and phase of vibration at pilot seat (B). The prediction captures the trend of vibration magnitude and phase quite well with flight test. The change in vibration magnitude for the pitch-control link bearing fault is much smaller than that of

other faults. The reason is that for flight safety consideration the component fault is kept at a very low value.

Figures 23 shows blade-tip flap and lag deviations between the faulty blade and others at 180-deg azimuth angle. Both prediction and flight-test results show that the tip displacement deviations are small. And they are not sensitive to flight-speed change.

Conclusions

The ability to analytically predict the effects of rotor-system faults on fuselage vibrations is very challenging. Not only is a sophisticated rotor-system model with the capability to represent dissimilarities required, but the rotor model must also be coupled to an accurate fuselage model. This paper describes an analytical model that integrates all of the required elements into a fully coupled rotor-fuselage analysis. Several rotor-system faults are modeled. Airframe vibrations and blade responses are predicted in hover and forward-flight conditions. The predicted results are compared with actual flight-test data.

Based on this study, some observations are noted:

1) Bifilar vibration absorbers reduce the 4/rev vibration by reducing the 3/rev in-plane hub loads in the rotating system. Results indicate that in order to predict fuselage vibration correctly for the SH-60 helicopter bifilar vibration absorbers should be considered in the analytic model. However, bifilar absorbers have a small effect on the 1/rev vibration caused by rotor-system faults.

2) Root mass imbalance fault causes small blade-tip track deviations at 180-deg azimuth, and these deviations are insensitive to flight speed.

3) The magnitude of 1/rev fuselage vibration and blade-tip flap deviation at 180-deg azimuth caused by misadjusted trim-tab fault increases with flight speed.

4) Misadjusted pitch-control link fault causes significant tip track deviation at 180-deg azimuth.

5) Pitch-control link free-play fault causes small change in the magnitude of 1/rev vibration. It also causes small blade track height deviation at 180-deg azimuth, which is insensitive to flight speed. The reason for this is probably because the embedded fault was not significant enough.

References

[1]Ganguli, R., Chopra, I., and Haas, D. J., "Formulation of a Helicopter Rotor-System Damage Detection Methodology," *Journal of the American Helicopter Society*, Vol. 41, No. 4, 1996, pp. 302–312.

[2]Ganguli, R., Chopra, I., and Haas, D. J., "Helicopter Rotor System Fault Detection Using Physics-Based Model and Neural Networks," *AIAA Journal*, Vol. 36, No. 6, 1998, pp. 1078–1086.

[3]Ganguli, R., Chopra, I., and Haas, D. J., "Simulation of Helicopter Rotor-System Structural Damage, Blade Mistracking, Friction and Freeplay," *Journal of Aircraft*, Vol. 35, No. 4, 1998, pp. 591–597.

[4]Ganguli, R., Chopra, I., and Haas, D. J., "Simulation and Detection of Rotor-System Faults Using Neural Networks," *Journal of the American Helicopter Society*, Vol. 42, No. 2, 1997, pp. 161–171.

[5]Azzam, H., and Andrew, M. J., "The Use of Math-Dynamic Models to Aid the Development of Integrated Health and Usage Monitoring System," *Journal of Aerospace Engineering*, Part G, Vol. 206, No. 1, 1992, pp. 71–96.

[6]Azzam, H., "The Use of Mathematical Models and Artificial Intelligence Techniques to Improve HUMS Prediction Capabilities," *Proceedings of the Royal Aeronautical Society Innovation in Rotorcraft Technology Conference*, The Royal Aeronautical Society, London, UK, 1997, pp. 16.1–16.14.

[7]Wallace, M., and Azzam, H., "Development and Use of A Finite Element Model to Investigate the Relationship Between Helicopter Hub Loads and Airframe Stresses," *Proceedings of 1999 MSC Users' Conference*, MSC Software, Los Angeless, 1999.

[8]Hansford, R. E., and Vorwald, J., "Dynamics Workshop on Rotor Vibratory Loads Prediction," *Journal of the American Helicopter Society*, Vol. 43, No. 1, 1998, pp. 76–87.

[9]Yeo, H., and Chopra, I., "Effects of Modeling Refinements on Coupled Rotor/Fuselage Vibration Analysis," *Journal of Aircraft*, Vol. 38, No. 1, 2001, pp. 111–121.

[10]Yeo, H., and Chopra, I., "Coupled Rotor/Fuselage Vibration Analysis Using Detailed 3-D Airframe Models," *Mathematical and Computer Modeling*, Vol. 33, May 2001, pp. 1035–1054.

[11]Bagai, A., and Leishman, J. G., "Rotor Free-Wake Modeling Using a Pseudo-Implicit Relaxation Algorithm," *Journal of Aircraft*, Vol. 32, No. 6, 1995, pp. 1276–1285.

[12]Bir, G., Chopra, I., Ganguli, R., Smith, E. C., Vellaichamy, S., Wang, J., Kim, K. C., Chan, W. Y., Nixon, M. W., Kimata, N. W., Smith, J. A., Torok, M., and Nguyen, K., "University of Maryland Advanced Rotorcraft Code (UMARC) Theory Manual," Univ. of Maryland, UM-AERO Rept. 94-18, College Park, MD, July 1994.

[13]Paul, W. F., "Development and Evaluation of the Main Rotor Bifilar Absorber," *Proceedings of the 25th American Helicopter Society Annual Forum*, The American Helicopter Society, Alexandria, VA, 1969.

[14]Den, Hartog, J. P., *Mechanical Vibrations*, McGraw–Hill, New York, 1956, pp. 219–222.

[15]Abbot, I, H., and Von Doenhoff, A. E., *Theory of Wing Sections*, Dover, New York, 1959, pp. 188–200.

[16]Haas, D. J., and Schaefer, C. G., Jr., "Air Vehicle Diagnostic System Technology Demonstration Program," *Proceedings of the 55th American Helicopter Society Annual Forum*, The American Helicopter Society, Alexandria, VA, 1999, pp. 2357–2372.